Simulating the levitation of Pyrolytic graphite above an array of N42 neodymium permanent magnets to study diamagnetic levitation

Christian Jarjat

Department of Physics, University of Bath, Bath, BA2 7AY, UK
Date submitted 10th May 2022

Abstract

Creating a simulation of pyrolytic graphite levitating in a magnetic field generated by an array of N42 neodymium permanent magnets to study diamagnetic levitation. By using experiments to measure the properties of these objects, the simulation could accurately calculate the stable levitation height as to agree with the physically measured results. The diamagnet's levitation height was found to be dependent on its orientation relative to the magnet array and its surface area. This added to the already established factors: diamagnet's magnetic susceptibility, the strength of the magnetic field and the diamagnet's position in the magnetic field. For stable diamagnetic levitation to occur, two requirements were found. First, the magnet array needs to be arranged so that it creates an area of zero vertical magnetic flux density above the array. Second, the diamagnet needs to be in a shape with an even order of rotational symmetry, as to a have zero torque about the horizontal axes.

1. Introduction

Materials are comprised of magnetic moments, $\vec{\mu}$ [1][2][3]. These can form in two ways: the orbit of electrons and their spin, each reacting differently to external magnetic fields, $\vec{H}$ [1][2][3]. Spin magnetic moments align themselves parallel to $\vec{H}$, amplifying the field inside the material and experiencing paramagnetism. While the orbital magnetic moments will increase or decrease as to oppose $\vec{H}$, due to Lenz's law [2], and experience diamagnetism.

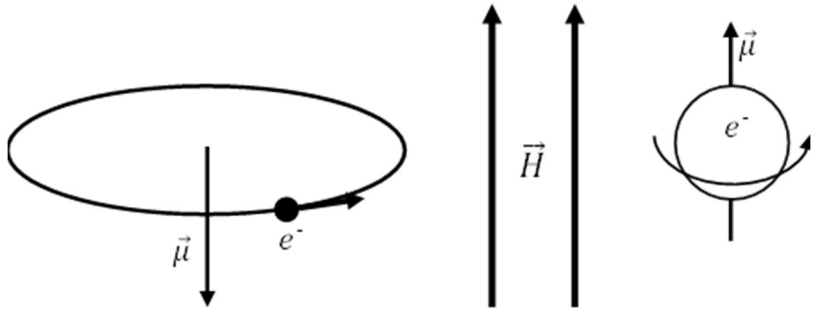

Figure 1: Two magnetic moments, orbital moment (left) and the spin moment (right), reacting to an external magnetic field.

Over the whole material, the density of magnetic moments, also known as the magnetization, can be calculated by

$$\vec{M} = \vec{\chi} \cdot \vec{H} = \frac{1}{\mu_0} \vec{\chi} \cdot \vec{B}, \tag{1}$$

where

$$\vec{M} = \frac{\vec{\mu}}{V}, \tag{2}$$

where $\vec{M}$ is the magnetization of the material, μ_0 is the vacuum permeability, $\vec{B}$ is the magnetic flux density of the external magnetic field, V is the volume of the material and $\vec{\chi}$ is the magnetic susceptibility tensor of the material [1]. $\vec{\chi}$ determines the strength and type of the magnetic response [1]. It is a dimensionless tensor, as due to a material's atomic structure, it can have different magnitudes of magnetic response, depending on the direction of $\vec{B}$ [4]. If $\vec{\chi}$ is positive, the material's magnetic response is primarily paramagnetic, while if it were negative, it would be classed as a diamagnet.

There are two main factors that determine if a material exhibits substantial diamagnetism [1][2]. First is if it has paired, covalent electrons, as the opposite spins in the pair will cause a net zero spin magnetic moments created. The second is if it has a high conductively due to having delocalised electrons. These free electrons form large orbits throughout the material, creating a larger magnetic moment than if they were just orbiting a nucleus.

Magnetic fields exert a repulsive force onto these diamagnets, given by

$$\vec{F}_m = V(\vec{M} \cdot \vec{\nabla})\vec{B} = \frac{V}{2\mu_0}(\vec{\chi} \cdot \vec{\nabla}B^2), \tag{3}$$

where $\vec{F}_m$ is the diamagnetic force[1]. If this is large enough, and is aligned antiparallel to the object's weight by

$$\vec{F}_w = \rho V g, \tag{4}$$

where ρ is the density of the material and g is the acceleration due to gravity, it can levitate in the magnetic field [1][5]. Substituting equation (3) into (2) will give the condition for levitating as by

$$\rho g = \frac{\chi_z}{2\mu_0} \frac{d(B^2)}{dz}, \tag{5}$$

where χ_z is the magnetic susceptibility of the object when $\vec{B}$ is aligned antiparallel to the object's weight, B^2 the square of the magnitude of the magnetic flux density squared, and z is the distance in the direction antiparallel to the object's weight. Equation (4) shows that any diamagnetic material will levitate in a magnetic field provided there is a strong enough magnetic field, this includes living creatures, such as the frog in figure 2 as the water inside it is diamagnetic [6].

Diamagnetic levitation has many applications. One such is in calibrating atomic force microscopes (AFM) [7]. A diamagnet can be placed inside an AFM and subjected to a magnetic field generated by permanent magnet array. The $\vec{F}_m$ induced can be measured by the microscope and compared to $\vec{F}_m$ calculated by equation (2). Another application is in Microrobotics [8]. If microrobots are constructed with diamagnetic material, they can be actuated by external magnetic fields. This allows them to be controlled in isolated environments where conventional means of control are difficult or dangerous, such as using microrobots in surgery that would be invasive otherwise.

The perfect material to levitate are superconductors, which have a χ_z of -1. However, they require to be in ultra-low temperatures to maintain the superconducting state, which can be

difficult and expensive [9]. The most practical objects that display significant levitation, are ones with a low density and a large, negative $\vec{\chi}$ at easily achievable temperatures. One such material is pyrolytic graphite, it has a large, negative $\vec{\chi}$ at room temperature due to its high conductivity [10]. Additionally, it has a relatively low density, making it able to levitate in magnetic fields, even in fields created by arrays of permanent magnets.

Figure 2: Frog levitating in Magnetic Field of Flux density 16T [6]

2. Computational Methods

To study the graphite's diamagnetic levitation, a simulation was constructed. First, a Cartesian grid was created, with each axis being in meters. Throughout the paper, the "horizontal axis" references either the x or y axis, while the "vertical axis" references the z axis. Then, the permanent magnets were placed in the grid so that the origin is above the centre of the magnet array and sits on its top surface. This made any distance in the positive z direction the distance from the magnet's surface.

Each magnet was subdivided into small cubic sections with a length of 0.4mm, each with a position vector relative to the grid, $\overrightarrow{r_m}$, and its own magnetic moment, $\overrightarrow{\mu_m}$, in the direction of its magnet's $\vec{B}$. After that, the graphite was placed in the grid. Like the magnets, it was split into smaller composite sections. It was split into ten parts in the x and y direction and three parts in the z direction, each section having its own volume and position vector, $\overrightarrow{r_g}$. This overall increased the accuracy of the simulation, as it better factored in the size and shape of the objects, rather than treating them as a point particle. The graphite could be moved and rotated throughout the grid, allowing the study of the levitation. However, the magnets were fixed in their position once they were placed in the grid.

The magnetic flux density due to a magnet section's $\overrightarrow{\mu_m}$, was calculated at the position of a section of graphite from

$$\vec{B}_m = \mu_0 \frac{3\vec{r}(\overrightarrow{\mu_m} \cdot \vec{r}) - \overrightarrow{\mu_m}|\vec{r}|^2}{4\pi|\vec{r}|^5}, \tag{6}$$

with

$$\vec{r} = \overrightarrow{r_g} - \overrightarrow{r_m}, \tag{7}$$

where $\vec{r}$ is the position vector from the magnet section to the graphite section, and $\vec{B}_m$ is the magnetic flux density due to the magnet section [2]. Summing the contributions of $\vec{B}_m$ from all the magnet sections gave the total magnetic flux density from the magnet array, at that graphite section position, $\vec{B}$.

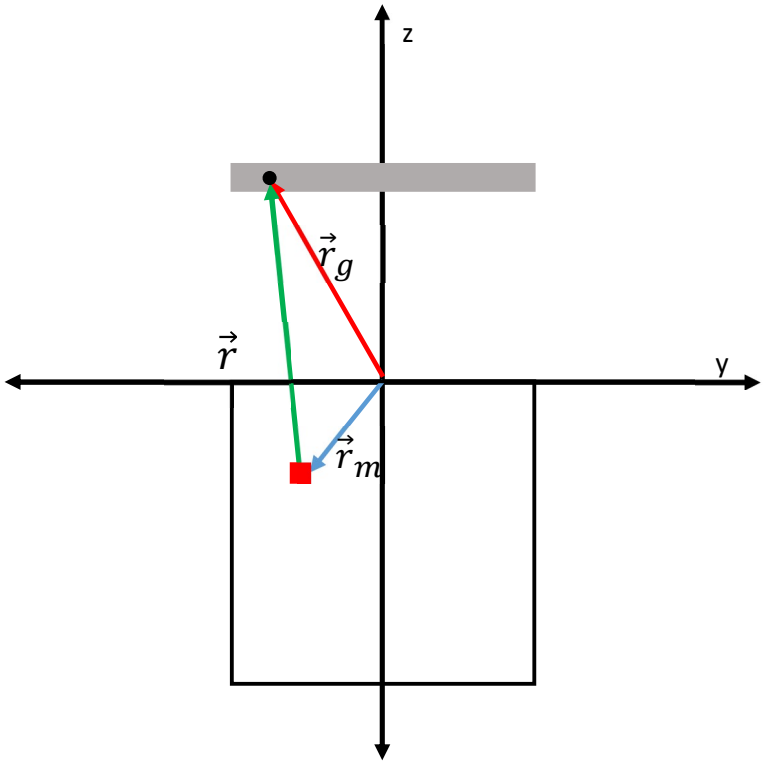

Figure 3: An iteration of calculating $\vec{B}$ for a single magnet at the position of a graphite section, the black dot, in the xz-plane. The red square is the magnet section where $\vec{B}$ is being calculated. The coloured arrows are the position vectors of: $\vec{r}_m$ (blue), $\vec{r}_g$ (red) and $\vec{r}$ (green).

With $\vec{B}$ calculated for every graphite section, the diamagnetic energy and force could be calculated for each section. Equation (2) was used to calculate the force while the diamagnetic energy was given by

$$E_m = -V_s \vec{M} \cdot \vec{B}, \tag{8}$$

where E_m is the diamagnetic energy of the graphite section and V_s is the volume of the graphite section [1]. The gradient in equation (2) was estimeated with centred-difference approximation [11].

3. Equipment

Figure (4) shows the magnets and graphite used for the levitation. The permanent magnets were N42 neodymium cube magnets. In the direction perpendicular to $\vec{B}$, there is a 2mm diameter hole through the magnet, allowing them to be secured in arrays by inserting insulating rods. To account for the hole in the simulation, the magnet sections that had the same position as the hole were removed, making the simulated magnetic field more accurately line up with the physical field. For consistently, the hole in the magnets was always parallel to the grid's y axis. The pyrolytic graphite was a thin sheet in the shape of a square.

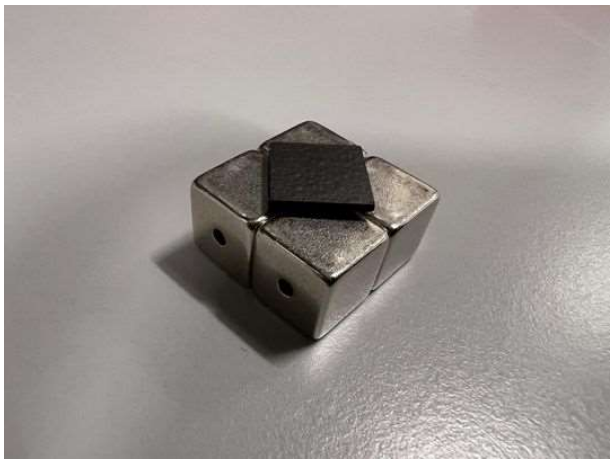

Figure 4: Pyrolytic graphite in stable levitation above a 2x2 array of N42 neodymium permanent magnets [12].

3.1 Masses and Physical Dimensions

Their physical dimensions were measured using a micrometre screw gauge, while their masses were measures using a digital weighing balance, with an insulating layer to reduce the effect of magnetic fields from the permanent magnets.

Table 1: The masses in grams, the length and thickness in millimetres of the permanent magnets and graphite used in the levitation and simulation.

	Mass / g	Length / mm	Thickness / mm
Permanent Magnet	7.087± 0.014	9.982± 0.021	
Pyrolytic Graphite	0.242± 0.001	10.376± 0.012	1.048± 0.004

3.2 Magnet's Magnetisation

A crucial property the simulation needed was $\overrightarrow{\mu_m}$. This could be easily calculated by finding the magnetisation of the permanent magnets, $\overrightarrow{M_m}$, and using equation (2). The magnets generate a permanent magnetic field because they are ferromagnetic [13]. Unlike diamagnets or paramagnets, the dipoles of a ferromagnet are always aligned, even when they are not in a $\vec{H}$. Due to this, equation (1) does not hold, as $\overrightarrow{M_m}$ non-zero in no magnetic field. However, when $\vec{H}$ is small, it is still proportional to any changes in $\overrightarrow{M_m}$.

To measure $\overrightarrow{M_m}$, a pair of Helmholtz coils were used to create a uniform magnetic field so that a permanent magnet can harmonically oscillate in it [14]. The magnitude of the magnetic flux density, B,at the centre of the two coils, is given by

$$B = \frac{{R_c}^2 \mu_0 N i}{\left({R_c}^2 + \left(\frac{D}{2}\right)^2\right)^{\frac{3}{2}}}, \tag{9}$$

where R_c is the radius of the coil, D is the distance between the two coils, N is the number of turns in each coil, i is the current through the coils and μ_0 is the Vacuum permeability [14]. Placing a permanent magnet in between the coils made it align its $\overrightarrow{\mu_m}$ parallel to the coil's $\vec{B}$. When the magnet was displaced by a small angle on the axis parallel to $\vec{B}$, as seen in figure 5, a torque is applied to return it to the initial aligned position. This created a harmonic oscillation, which could be modelled by Newton's second law for rotation in

$$\tau_r = I\frac{d^2\varphi}{dt^2} = C\varphi + V_m M_m B sin\varphi, \tag{10}$$

where τ_r is the rotational torque of the magnet, V_m is the volume of the permanent magnet, I is the moment of inertia of the magnet, t is time, φ is the displacement angle and C is a constant [5]. By using the small angle approximation and solving the differential equation (10), the rotational oscillation period, T, can be related to B in

$$\frac{2\pi}{T} = \sqrt{\frac{C + M_m V_m B}{I}}, \tag{11}$$

[15]. However, due to the nature of the permanent magnets, B must stay relatively small to keep M_m at a constant value [13].

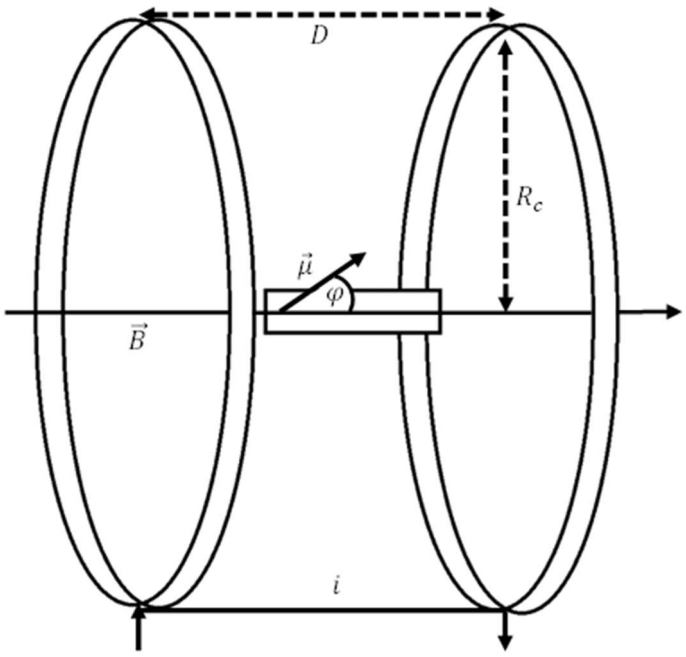

Figure 5: A permanent magnet in between two Helmholtz coils, oscillating in the direction of the $\vec{B}$.

The apparatus was set up as in figure 6. The current, i, was varied using the power supply and measured using the multimeter. The oscillations of the permanent magnets were recorded using a high-speed camera, then by using video editing and viewing software, T was measured. To reduce error in determining a complete oscillation, three magnets were used in series instead of just a singular magnet, as I increases so does T. The total moment of inertia for the array was estimated by

$$I = \frac{3\rho_m a^3}{16}(12a^2 - d^2), \tag{12}$$

where ρ_m is the mass density of the magnets, a is the length of a single magnet, and d is the diameter of the hole in the magnet [16].

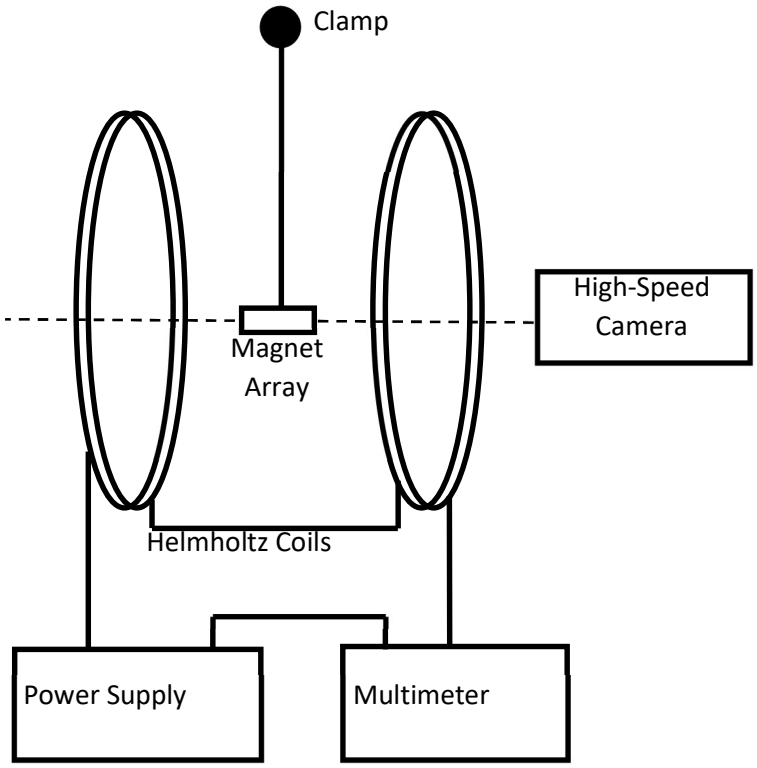

Figure 6: Diagram of a magnet array suspended, by a clamp piece, in between two Helmholtz coils. A power supply and a multimeter are in series with the two coils. A highspeed camera is positioned facing the magnet array beyond the front coil.

$(2\pi/T)^2$ was plotted against B. M_m was calculated by multiplying the gradient of the line of best fit in figure 7 by I and dividing by V_m. came to be $(1.06 \pm 0.07)x10^6$ Am^{-1}. The main source of error came from measuring the period. What determined a full cycle proved challenging to keep consistent. However, the precautions that were put in place reduced this error to an acceptable amount.

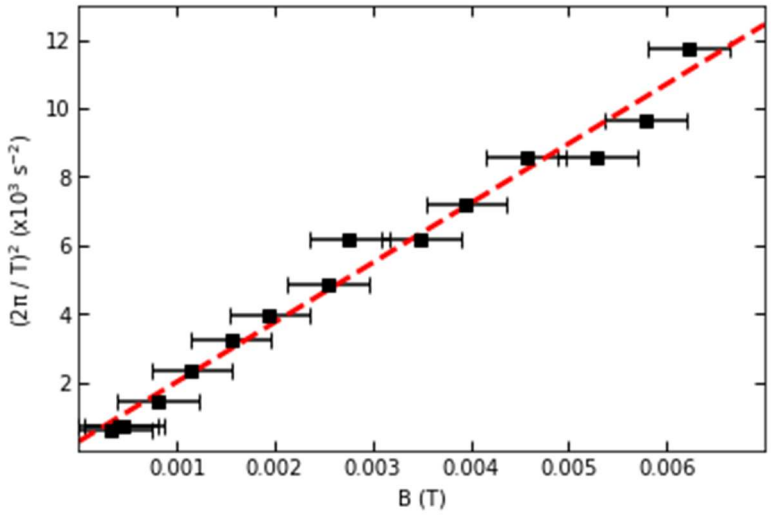

Figure 7: A graph of $(2\pi/T)^2$ against $\vec{B}$, with the black squares as the data, the black solid lines as the error, and the red dotted line as the line of best fit

3.3 Graphite's magnetic susceptibilities

Pyrolytic graphite is constructed of layers of carbon atoms, covalently bonded together in a 2D hexagonal Bravais lattice [10]. These layers are then held together by the interaction between the layers and delocalised electrons. Due to this atomic structure, pyrolytic graphite has two significant $\vec{\chi}$ terms. One where $\vec{B}$ is parallel to the graphite's carbon layers, χ_H, and one where it is perpendicular to its carbon layers, χ_V [17]. During levitation, the graphite's carbon layers are parallel to the horizontal axes, so χ_V is used for χ_z in equation (5) to determine the condition for levitation.

Table II: The parallel and perpendicular $\vec{\chi}$ terms for pyrolytic graphite [17].

	$\chi(x10^{-6})$
χ_H	-85
χ_V	-450

To test the purity of the graphite being used, χ_V was calculated by measuring the diamagnetic force with a digital weighing balance [18]. If the graphite and magnet array in levitation were inverted, so that the magnet array is above the graphite, $\vec{F}_m$ induced will be parallel to the graphite's weight. This is equivalent to increasing the graphite's mass, thus increasing its weight. Consequently, if the graphite were siting on a weighing scale, the difference in mass measured, when a magnet array is over the graphite and when not, can be used to calculate χ_V. Rearranging equation (5) and substituting in the mass change and volume gave

$$\chi_v = \frac{2\mu_0 \Delta m g}{V} \left(\frac{d(B^2)}{dz}\right)^{-1}, \tag{13}$$

where Δm is the change in mass of the graphite [18].

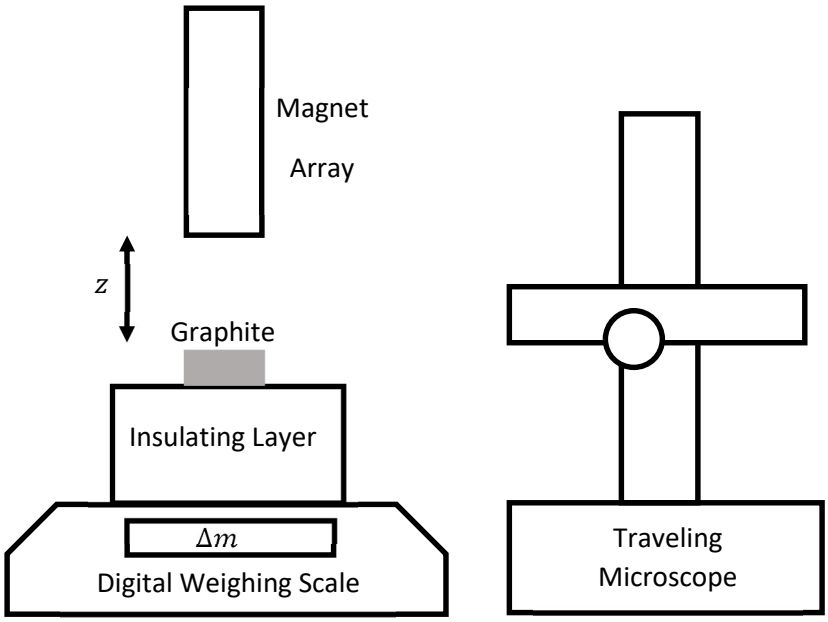

Figure 8: Diagram of a piece of graphite on a digital weighing balance, on top of insulation. A magnet array attached to a clamp's arm is above it. A traveling microscope is used to measure the height between the graphite and magnet array.

The apparatus was set up as in figure 8. The magnet array was comprised of three magnets in series, as to hold the array more easily in the clamp. By moving the clamp's arm, the magnet array could be positioned either above the graphite, or away from it. The graphite sat on an insulating layer to reduce the effect the magnetic fields had on the digital weighing scale when the magnets were above it. To measure the height between the magnet array and graphite, a traveling microscope was used each time to measure the heights of the bottom of the magnet array and the top surface of the graphite. The gradient of B^2 was calculated using the simulation. Δm was measured multiple times at different heights above the graphite.

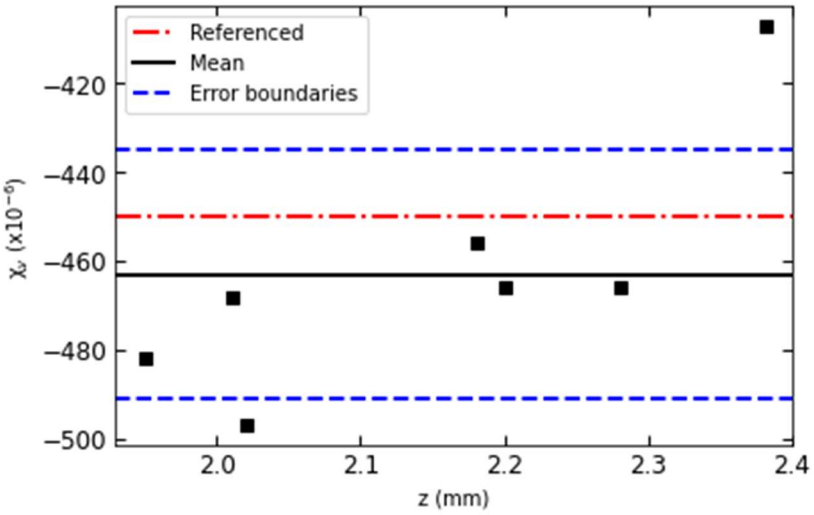

Figure 9: A graph of χ_V against magnet array height, with the black square as the data, the black solid line as the mean χ_V, the blue dotted lines as the error bounds of the mean χ_V, and the red dotted line as the referenced χ_V from table I.

The χ_V calculated for the different magnet array heights were plotted against each other in figure 9. The mean χ_V came to $-463 \pm 28\, x10^{-6}$, with the majority of the χ_V calculated within one error bound. This agrees with the referenced value of χ_V in table I, suggesting the graphite is pure enough to use both referenced values, χ_V and χ_H in the simulation. The main source of error were outside vibrations affecting the weighing scale. Due to the small mass of the graphite, Δm was small enough for the vibrations to cause a significant percentage variation in the weight measured. To reduce this error as much as possible, the experiment was done in an isolated environment.

4. Simulating Magnet Array

4.1 Single Magnet

For the simulation function correctly, the magnetic field generated by the code needs to agree with the field generated by the real, permanent magnets. First, the z component of $\vec{B}$ (B_z) of a permanent magnet was measured using a Hall probe and a micro positioner, as shown in figure 10. The Hall probe was moved across equally spaced points along the surface of the magnet and at a height of 2mm above it [18]. This created two surfaces of physically measured B_z readings. Then, $\vec{B}$ was calculated for an array of coordinate points in the xy-plane at the same two heights as the measured B_z readings, the surface and 2mm above the array. This created two surfaces of simulated B_z.

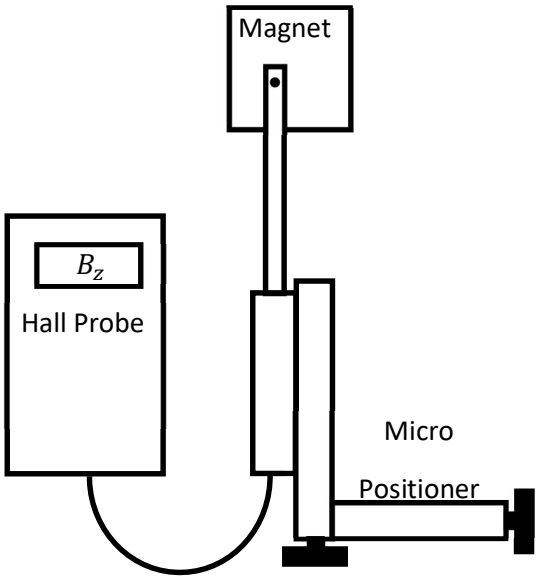

Figure 10: Diagram of top-down view of a hall probe attached to a micro positioner, mapping B_z of a single magnet at different heights above its surface.

Figure 11a shows that B_z at the surface of the magnet is uniform, with a large drop off past the edges of the surface. While at 2mm above the surface, as shown in figure 11c, the surface begins to curve into a paraboloid, with the point above the magnet's centre as the maximum [19]. The percentage differences between the physically measured and simulated B_z were plotted for both heights in figures 11b and 11d. The only significant difference between the measurements and simulation are the points above the entrances of the magnet's hole at the surface map, with a disparity of 8% from the measured value. The rest of simulated values show negligible differences between the measured values. This may be due to 2mm being much larger compared to the distance between each of the simulated magnet sections, effectively making the magnet function as a single dipole at a far enough distance. As the graphite is

levitating in between these heights, the simulation can be deemed accurate enough to simulate magnetic fields, with a percentage error of 0.25% for the simulated $\vec{B}$.

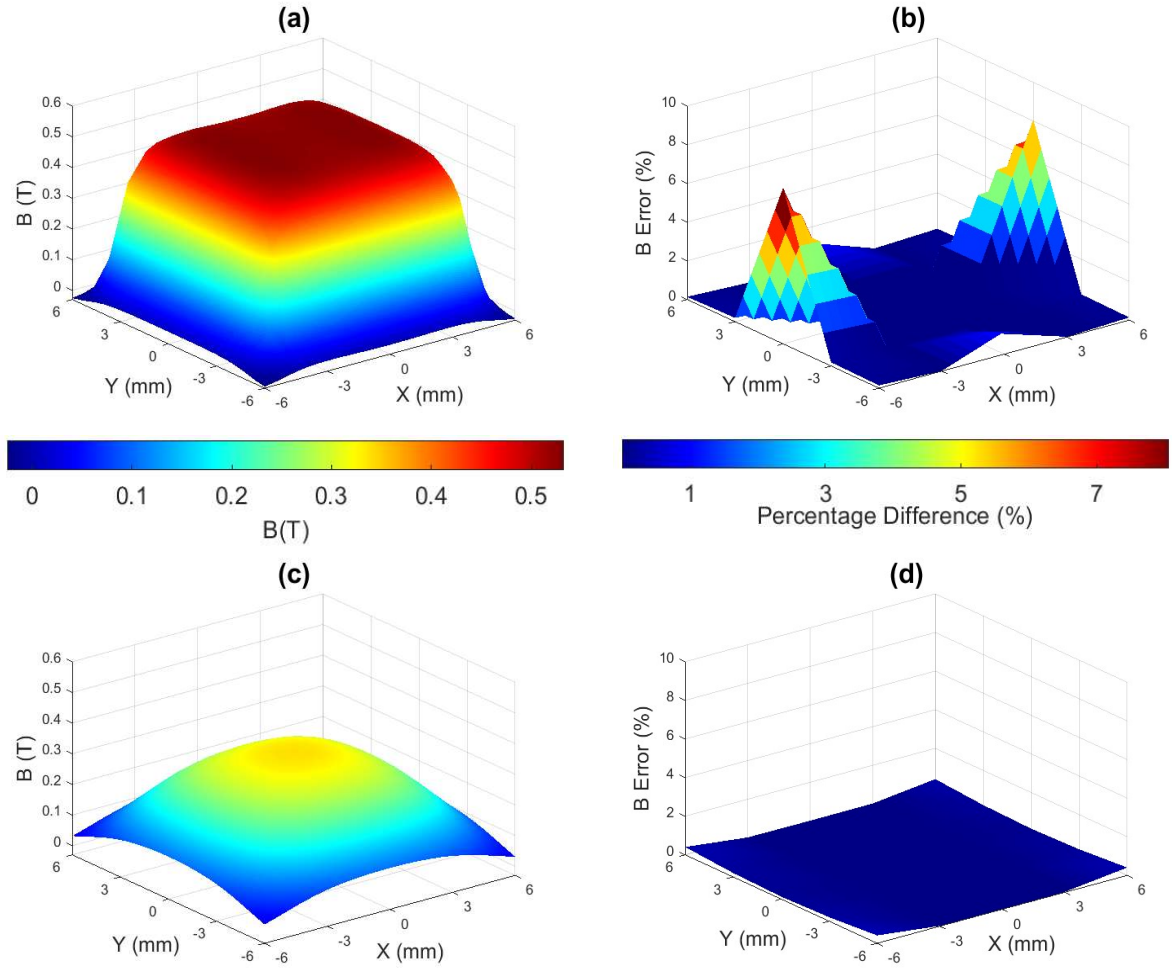

Figure 11: simulated B_z at (a) the surface and (c) 2mm above the surface of a single magnet, with the centre of the top surface at the origin. And the percentage differences between the simulated B_z and the measured $B_z$at (b) the surface and (d) 2mm above the surface of the magnet.

4.2 2x2 Magnet Array

The simplest magnet array that supported stable levitation for our graphite was a 2x2 array, with the alternating poles, as seen in figure 4. B_z was mapped for the surface of the array and 2mm above the surface in figure 12. As for the single magnet in figure 11a, the magnet array created a uniform field at its surface, with it only changing at the boundaries between the separate magnets. While in at 2mm above the surface, the same paraboloid shape forms at the centre of each magnet in the array.

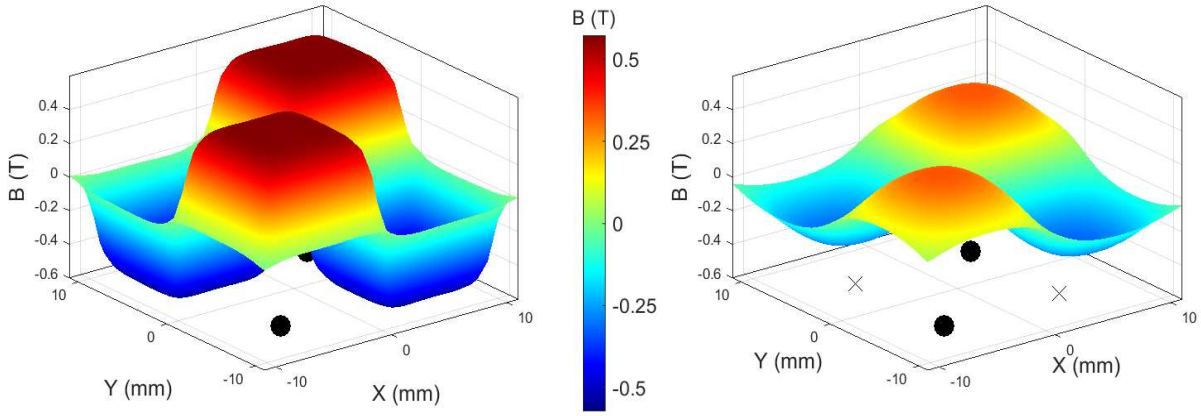

Figure 12: B_z at the surface (left) and 2mm above the surface (right) of a 2x2 magnet array, with the centre of the top surface at the origin. The dots (positive) and cross (negative) shows the direction of magnet's poles in the z direction.

To get a more detailed representation of the magnetic field created by the array, all three components of $\vec{B}$ are shown in figures 13a-13c. The horizontal components of $\vec{B}$, B_x and B_y for the x and y axis respectively, are concentrated above the boundaries between the magnets, figures 13a and 13b. They have an overall direction towards the two south poles of the array, signifying the magnetic field at these boundaries curve, traveling from the north to the south poles. This explains the reduced B_z above the boundaries in figure 13c, the field is changing direction and thus reducing its z component. This creates points of zero B_z above the boundaries of the magnets in the array.

Figure 13d-13f shows the diamagnetic force density, $\vec{f}_m$ induced by the magnetic field from the array, over a graphite section at that point. The x and y components of $\vec{f}_m$ (Figures 13d-13e) near the array edge boundaries are pointing away from the array. This will push the graphite off the array if it gets close enough to the edges. This is the same for the boundaries between the magnets, however due to the neighbouring magnets having opposite polarities, the two forces cancel out. This leaves a cross-shaped area of zero horizontal force over the inside magnet boundaries.

The z component of the $\vec{f}_m$ (figure 13f) shows a positive vertical force across most of the array. This is explained by equation (3), $\vec{F}_m$ is proportional to the gradient of B^2. This makes the direction of the magnetic field irrelevant in determining the direction of $\vec{F}_m$, it is parallel to the direction of decreasing magnitudes of magnetic field strength. So, even though the graphite sections above the north pole magnets have their magnetic moments pointing downwards, the force induced still acts antiparallel to its weight as B^2 decreases with vertical height.

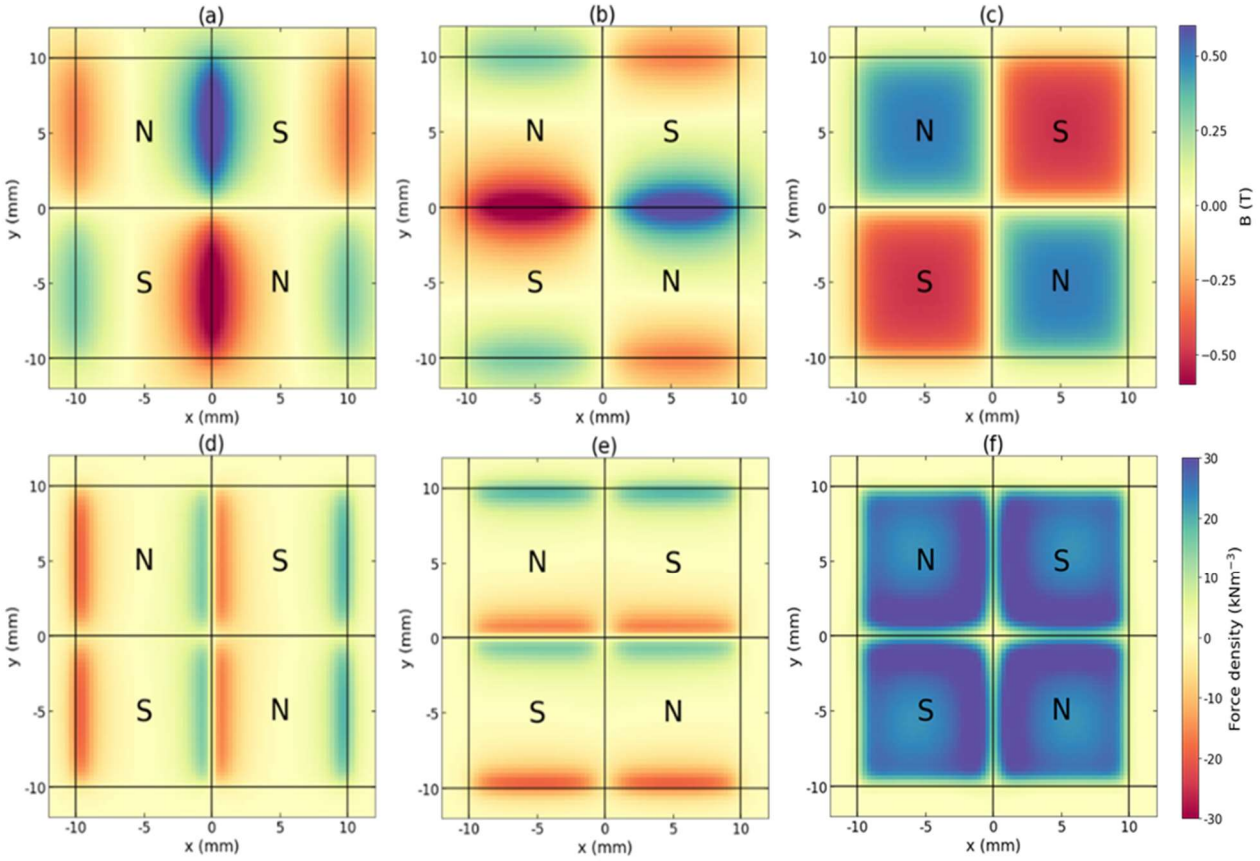

Figure 13: At a height of 1mm above the surface of the 2x2 magnet array, the compounds of $\vec{B}$ in the x(a), y(b) and z(c) direction and the compounds of the force density in the x(d), y(e) and z(f) direction plotted on a heat map. The poles are labelled at the centre of each of the magnets in the array.

5. Stable Levitation

5.1 Measuring Stable Levitation Height

The levitation height was measured rudimentarily with a travelling microscope, as seen in figure 14. The height of the magnet array's top surface and the bottom of the graphite were measured on a veneer scale, then subtracted from each other to get the levitation height. This method had a great amount of error, as the microscopes available lacked any ability to vertically move in fine increments, such as an adjustment knob. They only relied on manually sliding it with your hand, which made it prone to slip while reading the veneer scale. However, after many repeated readings to reduce error, it gave an estimate of (1.27 ± 0.08) mm for the levitation height above the 2x2 array.

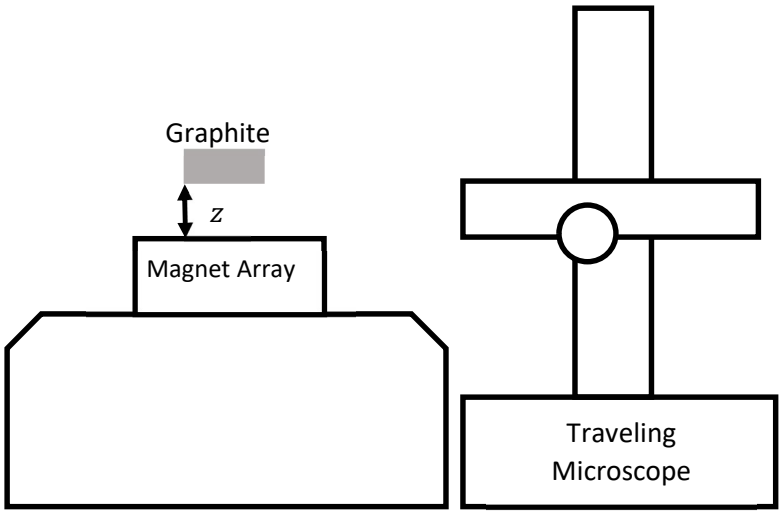

Figure 14: Diagram of a travelling microscope measuring the diamagnetic levitation height

5.2 Simulating at 0°

The simulation created the array in figure 4 and placed the graphite piece in the grid orientated at 0° relative to the magnet array in the xy-plane. Using equation (3) to calculate the $\vec{F}_m$ for each of the graphite sections, all the contributions in the z direction were summed together to give the total $\vec{F}_m$ on the graphite. Then, the solutions to equation (5) were numerically found using the Newton-Raphson method to an error of $\pm 5x10^{-4}mm$, giving the corresponding centre of mass coordinates where levitation occurs [20]. In equation (3), $\vec{F}_m$ is shown to depend on $\vec{B}$, which itself is dependent on the location above the magnet array. Therefore, each point in the xy-plane has a corresponding height where the graphite's centre of mass will be located when it is levitating. So, a surface of these levitation points is created when the graphite is aligned 0° relative to the magnet array. E_m of the whole graphite, using equation (8) and numerically integrating over the graphite's volume, was calculated at each of these levitation positions [21].

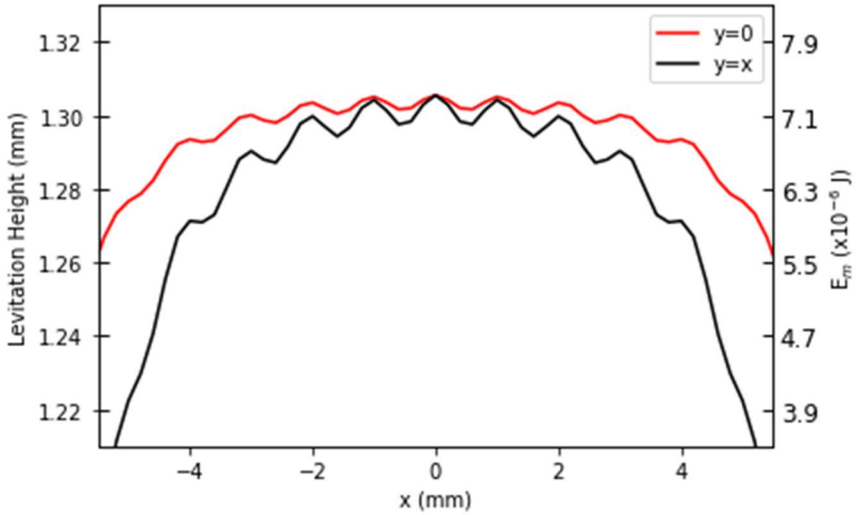

Figure 15: The levitation height and E_m of the graphite piece above a 2x2 magnet at a rotation of 0°, plotted against the coordinate of the graphite's centre of mass. The red line

is where the y coordinate equals 0, while the black line is where the y coordinate equals the x coordinate.

For the graphite piece to experience stable levitation at a point, it needs to minimise its magnetic energy [5]. If the piece is not at a minimum point, any small perturbation in the direction of negative E_m gradient will cause it to change its position. At an E_m minimum, small perturbations in any direction will create a restorative force towards the initial position, forming an energy well.

In figure 15, for both y=0 plane and y=x plane, there are many small minima near the centre of the magnet array, suggesting there are many stable levitation positions. The levitation height decreases dramatically when $|x| > 5mm$. This is due to parts of the graphite starting to levitate over beyond the edge of the array. As seen in figure 13, the z component of $\vec{F}_m$ is effectively zero for positions not directly above the array. So, as the graphite's centre of mass gets closer to the edge of the array, less of the graphite itself is contributing to total $\vec{F}_m$.

The E_m minima positions do agree with the height measured using the travelling microscope, being within the error range. However, when physically levitating the graphite there was only one stable levitation position, while the multiple minima suggest there are many stable positions. This is explained in figure 4, as when the graphite was in stable levitation, it was not aligned with the magnet array, rather it was orientated at an angle of 45°.

5.3 Energy Due to Rotation

E_m, when its centre of mass is above the centre of the array, was calculated as the graphite piece was rotated about the z axis using equation (8). The energy minima in figure 16 are at 45° and 135°, while the maxima are located at 0°, 90° and 180°. However, due to the graphite piece having a rotational symmetry of four, the minima and maxima angles have the graphite in the same orientation as each other. This confirms the favoured orientation for stable levitation, of the magnet array in figure 4, is at 45°.

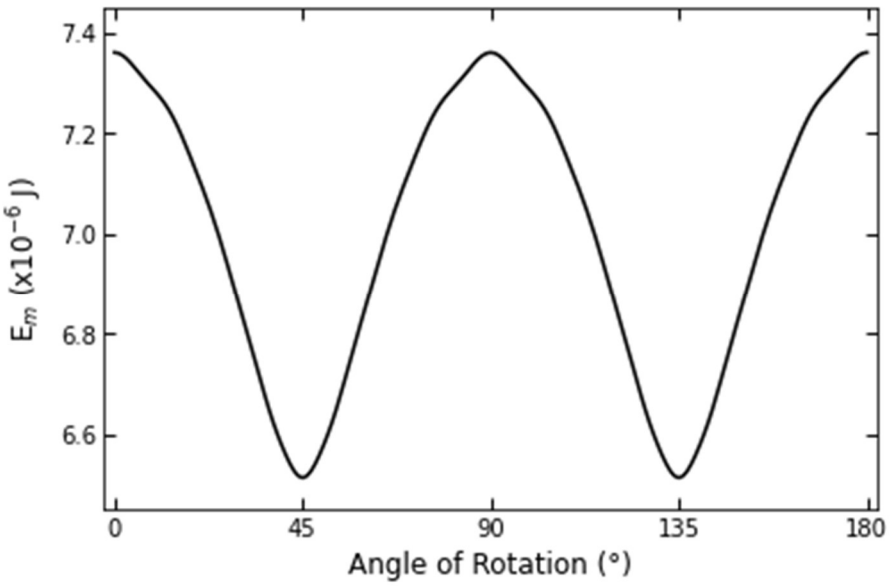

Figure 16: E_m plotted against the angle of rotation when the graphite, with its centre of mass above the magnet array's centre, is rotated about the z axis.

5.4 Torque Due to Rotation

Each graphite section experiences a different $\vec{F}_m$ compared to the neighbouring sections; some will experience a stronger $\vec{F}_m$ than others due the different $\vec{B}$ at each of the section's position. This creates a torque, as the imbalance of $\vec{F}_m$ cause the graphite to rotate [22]. The torque for each graphite section can be calculated by

$$\vec{\tau}_s = \overrightarrow{r_g} \times \vec{F}_m, \tag{14}$$

where $\vec{\tau}_s$ is the torque of the graphite section [22]. While the torque over the whole graphite piece ($\vec{\tau}$) was calculated by the numerical integration of all the graphite sections' contributions [21]. Similar to E_m, the components of $\vec{\tau}$ were calculated as the graphite piece was rotated about the z axis using equation (14).

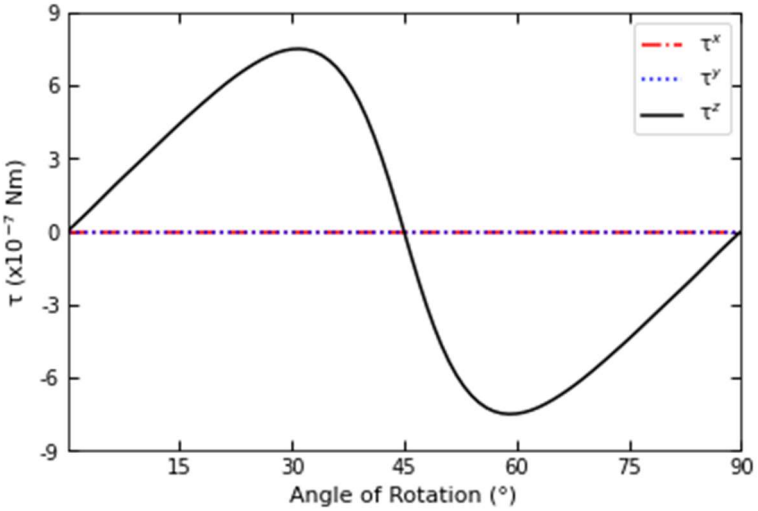

Figure 17: $\vec{\tau}$ plotted against the angle of rotation when the graphite, with its centre of mass above the magnet array's centre, is rotated about the z axis.

$\vec{\tau}$ that acts about the x and y axes, τ_x and τ_y, are zero for all angles, as seen in figure 18. This is due to the shape of the graphite having an even order rotational symmetry in the xy-plane. As the magnetic field produced by the magnet array is symmetric, $\vec{\tau}$ on one graphite section would be equal and opposite to $\vec{\tau}$ of a graphite section in its reflected position, as they will have the same $\vec{B}$ while their position vectors will be equal and opposite. This even symmetry allows stable levitation at the minimum point, as the graphite will not rotate about a horizontal axis and tip over. If the graphite's shape had an odd order of rotational symmetry, including shapes of order one, the torques about the horizontal axes would not balance. There would always be one side of the graphite that would experience a greater $\vec{\tau}$, as there are more graphite sections experiencing the diamagnetic forces than the opposite side.

The $\vec{\tau}$ about the z axis, τ_z, equals zero at the same angles as the E_m stationary points in figure 16. Any small perturbation in angle at the E_m maximums, where the τ_z gradient is positive, will cause an increased $\vec{\tau}$ in the perturbation's direction, accelerating the rotational motion away from the maximum's orientation. While any small perturbation in angle at the E_m minimums, where the τ_z gradient is negative, will cause a restorative motion towards the original orientation of the minimum, creating a stable alignment for levitation.

5.5 Simulating at 45°

The levitation height and E_m surface was computed for the graphite rotated at 45°. In figure 18, both, y=0 and y=x plane have a single E_m minimum, above the centre of the magnet array. This is positioned lower than the minima found for the graphite at 0° rotation, creating a deeper potential well and becoming the favoured levitation point at (1.2845 ± 0.0005)mm above the centre of the magnet array. This height agrees with the physical measurement and the observations, as there is only being a single stable levitation point. Thus, indicating that the stable levitation height is dependent on the orientation of the graphite, as well as its position in the magnetic field and its magnetic susceptibility.

The position of the stable levitation is also at the centre of a zero vertical force density area, as seen in figure 13f. Like for beyond the edge of the array, total vertical $\vec{F}_m$ decreases as less of the graphite is contributing to it. So, the graphite's total E_m is reduced as a result. This implies the magnet array needs to be arranged so that is has areas of zero B_z above the array, which causes the zero vertical $\vec{F}_m$ and allows the creation of an energy well.

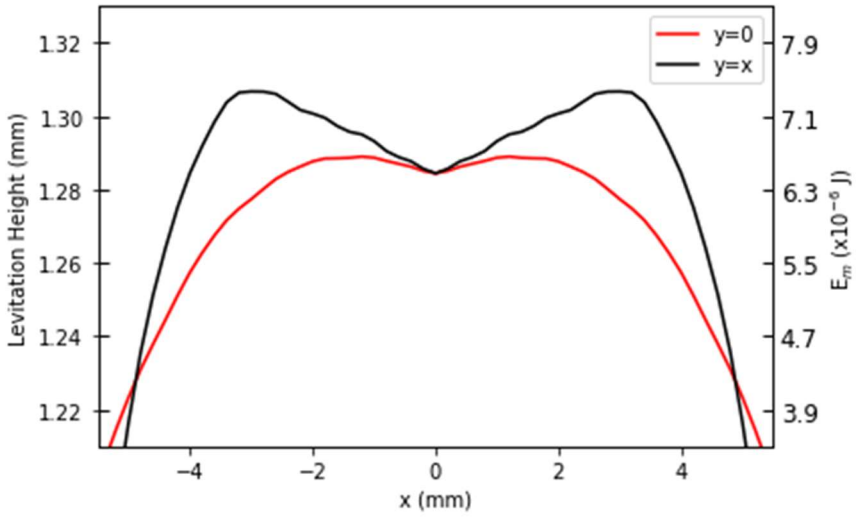

Figure 18: The levitation height and E_m of the graphite piece above a 2x2 magnet at a rotation of 45°, plotted against the coordinate of the graphite's centre of mass. The red line is where the y coordinate equals 0, while the black line is where the y coordinate equals the x coordinate.

6. Size Dependence

From equation (5), it shows a piece of graphite's levetaion is only dependant on its χ_z and the $\vec{B}$ it is in to levitate due to diamagnetism, while its volume is independent of it. However, as seen in the previous sections, stable levitation height depends on more variables. To test whether the graphite's volume, affects stable levitation, the stable levitation height was calculated for different lengths of the graphite piece, while keeping it at the same thickness as stated in table I. These were plotted in figure 19.

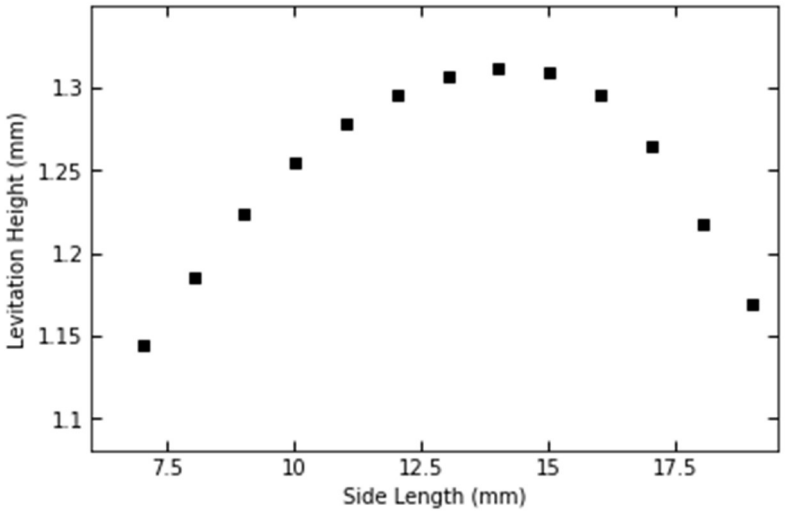

Figure 19: Stable Levitation height for different graphite sizes plotted against their side length.

As the graphite's surface area increases up to ~50% of the area of magnet array, the increased surface area increases the number of graphite sections. Therefore, there is a greater overall $\vec{F}_m$ acting on the graphite, allowing it to levitate higher. However, when the graphite increases it size past this threshold, the graphite's increasing weight surpasses the increase in $\vec{F}_m$. This is due to the finite magnetic field from the magnet array. The sections on the outer edge of the graphite experience a smaller $\vec{B}$ as the graphite's surface area increases, leading to a reducing rate of $\vec{F}_m$ increase over the whole graphite. The graphite's weight always increased as its size grew, as its weight is independent of $\vec{B}$. This trend indicates that for a given magnetic field generated by a magnet array, there is an optimal graphite surface area to achieve the maximum levitation height. For the array in figure 4, the optimal graphite surface area, while having the thickness stated in table I, is ~50% the magnet array's surface area.

7. Improvements

The major limiting factor to the accuracy of the simulation is the subdivision of the magnet and graphite into individual sections. To simulate the levitation, to a low enough degree of error, the sizes of the sections had to be very small. However, as the section size decreases, the number of total sections increased, each one computing the equations used through the study. As a result, the time taken to run a complete simulation exponentially increasing.

So, a balance of accuracy and efficiency had to be taken. If this study was repeated, with the completed simulation code, a smaller magnet section size would be chosen, at a sacrifice of computing time. This would reduce the spikes in percentage error seen in figure 11b, and better simulate the magnetic field nearer to the magnet's surface.

There are other aspects of the diamagnetic levitation simulation that could be studied in a follow-up study. Only one magnet array was simulated, more complex arrays could be created in the simulation, such as 3x3 or Halbach arrays [23]. This could lead to studying the effect the different arrays had on levitation and how to edit the array to increase the height of levitation. Simulating different shaped graphite pieces could test how $\vec{\tau}$ and E_m are affected by the different orders of rotational symmetry. Testing whether the even symmetry requirement holds for very large orders of rotational symmetry. Additionally, simulating diamagnetic materials in different states of matter, testing how diamagnetic force interact with fluid dynamics.

8. Conclusion

By using experiments to measure the properties of the N42 neodymium permeant magnets and the pyrolytic graphite, the simulation created was successful at modelling the graphite levitating. With the simulated levitation height agreeing with the physically measured height.

The diamagnet's levitation height is dependent on its magnetic susceptibility, it's orientation relative to the magnet array, the strength of the magnetic field generated by the magnet array, the diamagnet's position in the magnetic field, and the diamagnet's surface area.

For stable diamagnetic levitation to occur, there are two requirements. The magnet array needs to be arranged so that it creates an area of zero vertical magnetic flux density above the array. If the magnet array creates a symmetrical magnetic field, the diamagnet needs to be in a shape with an even order of rotational symmetry, as to a have zero torque about the horizontal axes.

9. Acknowledgments

I would like to thank my project partner, Adnan Siddiquei, for working with me in this project. As well, I want to thank our project supervisor, Dr Steve Andrews of University of Bath, for giving advice and answering questions related to the topic of our project. And finally, I would like to thank our lab Technician, Isabel Wells of University of Bath, for giving assistance in acquiring the equipment needed and the setup of physical experiments.

10. References

[1] Jiles D. Introduction to magnetism and magnetic materials. 2nd ed. London: CRC Press; 1998.

[2] Sadiku M. Elements of electromagnetics. 6th ed. Oxford: Oxford University Press; 2015.

[3] Griffiths D. Introduction to electrodynamics. 3rd ed. Upper Saddle River: Prentice Hall; 1999.

[4] Constable C, Tauxe L. The bootstrap for magnetic susceptibility tensors. Journal of Geophysical Research. 1990;95(B6):8383.

[5] Tipler P, Mosca G. Physics for scientists and engineers. 4th ed. New York: W.H. Freeman; 2000.

[6] Berry M, Geim A. Of flying frogs and levitrons. European Journal of Physics. 1997;18(4):307-313.

[7] Li Q, Kim K, Rydberg A. Lateral force calibration of an atomic force microscope with a diamagnetic levitation spring system. Review of Scientific Instruments. 2006;77(6):065105.

[8] Xu T, Yu J, Yan X, Choi H, Zhang L. Magnetic Actuation Based Motion Control for Microrobots: An Overview. Micromachines. 2015;6(9):1346-1364.

[9] Tinkham M. Introduction to superconductivity 2nd ed. Mineola, N.Y.: Dover Publications; 2004.

[10] Pierson H. Handbook of carbon, graphite, diamond, and fullerenes. Park Ridge, N.J: Noyes Publications; 2001.

[11] Wilmott P, Howison S, Dewynne J. Mathematical models of financial derivative products. New York: Cambridge University Press; 1995.

[12] Photo taken by project partner, Adnan Siddiquei

[13] Chikazumi S, Graham C, Chikazumi S. Physics of ferromagnetism. 2nd ed. Oxford: Oxford University Press; 1997.

[14] Barman B, Petrou A. Measuring the magnetization of a permanent magnet. American Journal of Physics. 2019;87(4):275-278.

[15] Holbrow C. Modern Introductory Physics. 2nd ed. New York, NY: Springer New York; 2010.
[16] Serway R. Physics for scientists and engineers. 2nd ed. Philadelphia: Saunders College Publishing; 1986.
[17] Simon M, Heflinger L, Geim A. Diamagnetically stabilized magnet levitation. American Journal of Physics. 2001;69(6):702-713.
[18] Laumann D, Heusler S. Determining magnetic susceptibilities of everyday materials using an electronic balance. American Journal of Physics. 2017;85(5):327-332.
[19] Encyclopedia Britannica, 2022. Paraboloid [Internet]. Available from: https://www.britannica.com/science/paraboloid [cited 10 May 2022].
[20] Râben'kij V, Tsynkov S. A theoretical introduction to numerical analysis. Boca Raton: Chapman & Hall/CRC; 2007.
[21] Davis P, Rabinowitz P. Methods of Numerical integration. London: Academic Press; 1975.
[22] Connolly J. Understanding the Magic of the Bicycle. San Rafael: Morgan & Claypool Publishers; 2017.
[23]]. Halbach K. Application of permanent magnets in accelerators and electron storage rings (invited). Journal of Applied Physics. 1985;57(8):3605-3608.